PERGAMON

International Journal of Heat and Mass Transfer 41 (1998) 3759–3769

International Journal of HEAT and MASS TRANSFER

Natural convection mass transfer along a dissolution boundary layer in an isothermal binary metallic system

S. W. Shiah[a,*], B. C. Yang[b], F. B. Cheung[c,†], Y. C. Shih[b]

[a] *Department of Naval Architecture and Marine Engineering, Chung Cheng Institute of Technology, Taoyuan, Taiwan, Republic of China*

[b] *Energy & Resource Laboratories, Industrial Technology Research Institute, Hsinchu, Taiwan, Republic of China*

[c] *Department of Mechanical Engineering, Pennsylvania State University, University Park, PA, U.S.A.*

Received 28 August 1997; in final form 2 March 1998

Abstract

The process of dissolution mass transport along a vertical soluble substrate submerged in a large pool of otherwise quiescent molten metal is studied theoretically. Various freestream concentrations varying from zero to a near-saturation value are considered. A mathematical model is developed from the conservation laws and thermodynamic principles, taking full account of the density variation in the dissolution boundary layer due to concentration differences, the influence of the solubility of the substrate on species transfer, and the motion of the solid/liquid interface at the dissolution front. The governing equations are solved by a combined analytical–numerical technique to determine the characteristics of the dissolution boundary layer. Based upon the numerical results, a correlation for the average Sherwood number is obtained. It is found that the Sherwood number depends strongly on the saturated concentration of the substrate at the moving dissolution front and the degree of saturation in the ambient pool.

Nomenclature

A degree of saturation in the ambient fluid
A_1, B_1 constants defined for the saturated concentration correlation, C_s
A_2, B_2 constants defined for the diffusion coefficient D
b_0, b_1, b_2 coefficients defined by eqn (32)
C local mass fraction of the substrate in the solution layer
$\tilde{C}$ modified local mass fraction of the substrate in the solution layer
C_s saturated concentration at the solid/liquid interface
$\tilde{C}_s$ modified saturated concentration at the solid/liquid interface
C_∞ ambient pool concentration
D mass diffusivity of the binary system
f unknown function of η
g acceleration due to gravity
Gr_x local Grashof number
Gr_L overall Grashof number
h_m local dissolution mass transfer coefficient
$\bar{h}_m$ average dissolution mass transfer coefficient
$\underline{Sc}$ Schmidt number
$\underline{Sh}$ average Sherwood number
Sh_0 average Sherwood number at the limits of $a \to 0$ and $C_s \to 0$
T_i solid/liquid interface temperature
T_{mp} melting point of aluminum
u velocity component in x-direction
v velocity component in y-direction
v_0 dissolution velocity defined by eqn (5c)
V_0 modified dissolution velocity defined by eqn (15d)
x, y coordinate axes
Y unknown function of a and C_s.

Greek symbols

δ dimensionless momentum boundary layer thickness
δ_c dimensionless concentration boundary layer thickness
η independent similarity variable

*Visiting Scholar, Department of Mechanical Engineering, The Pennsylvania State University, University Park, PA.

†Corresponding author.

0017–9310/98 $19.00
PII: S0017–9310(98)00096–9

ρ local density of the fluid
ρ_m molten metallic solvent density
ρ_s fluid density at the dissolution front
ρ_w soluble substrate wall density
ρ_∞ ambient fluid density
μ dynamic viscosity of the fluid
ν kinematic viscosity of the fluid
ψ functional form defined by eqn (28).

Subscripts
m molten metallic solvent
s saturation state
w the soluble substrate wall
∞ ambient fluid.

Superscript
n power index defined by eqn (29).

1. Introduction

The problem of dissolution of a vertical solid substrate in a molten metallic pool is of considerable practical importance in conjunction with the formation of alloys, casting of metals, corrosion of high-temperature containers, and safety analysis of advanced nuclear reactors [1]. In most cases, the density of the substrate is different from the density of the molten pool. As a binary solution is formed near the dissolution front, significant concentration-induced density gradients may develop in a region near the solid substrate. Under the influence of gravity, the concentration-induced density gradients create a strong buoyancy force which causes the dissolved material to move in the vertical direction, thus resulting in the development of a dissolution boundary layer. The boundary layer motion, in turn, enhances the local dissolution rate.

A dissolution boundary layer on a vertical substrate exhibits many unique features [2]. First, the boundary layer flow is concentration-driven rather than temperature-driven. Second, the fluid density is not a constant but varies locally with the concentration of the substrate. Although the fluid can be treated incompressible, the density variation in the dissolution boundary layer needs to be considered. Third, the solid/liquid interface is not fixed in space but is moving toward the interior of the substrate as dissolution proceeds. Finally, the maximum concentration of the substrate is limited by the saturation value at the system temperature. Thus the species transfer is strongly influenced by the solubility of the wall material. These unique features bring about a strong coupling of the hydrodynamic and transport process.

Very few studies of dissolution mass transport in liquid-metal systems have been performed in the past. Most works conducted by previous investigators in this area have been largely experimental, dealing either with the extent of dissolution subjected to given flow conditions [3–6] or with the composition of the alloy resulting from the dissolution process [7, 8]. Most recently, the fundamental aspects of the dissolution process and the dependence of the mass transport on the controlling parameters have been studied for a molten aluminum-steel system by Cheung et al. [1]. They performed a theoretical study of the behavior of a dissolution boundary layer on a vertical steel plate submerged in a pool of molten aluminum, accounting for various freestream velocities. However, their work was restricted to a single aluminum alloy system, i.e. Al–Fe system, with special emphasis on the effect of freestream velocity.

In this study, the characteristics of a dissolution boundary layer on a vertical metallic substrate submerged in a large pool of molten metal is investigated analytically. The problem is formulated using generalized expressions for the solubility and the mass diffusivity of the substrate such that the resulting governing system can be applied to any binary metallic systems. In addition, the effect of ambient pool concentrations is considered. A combined analytical-numerical technique is employed to solve the equations governing the dissolution mass transfer coefficient as a function of the controlling parameters of the system.

2. Mathematical model

A schematic of the physical system under consideration is shown in Fig. 1. The vertical soluble substrate having a density higher than the ambient fluid, is submerged in a large pool of otherwise quiescent molten metal. The dissolved material (i.e. the molten binary alloy) flows downward along the plate due to the effect of buoyancy as a result of concentration-induced density gradients within the solution layer. The system is considered isothermal (i.e. the substrate and the fluid are at the same temperature) during the dissolution process. To facilitate mathematical formulation of the problem, the dissolution process is treated to be steady and the dissolution front (i.e. solid/liquid interface) to remain vertical. These simplifications are deemed appropriate since the dissolution process is usually very slow owing to very small mass diffusivities for most binary metallic systems [10, 11]. The extent of wall erosion is small compared to the length of the plate. A two-dimensional Cartesian coordinate system moving with the dissolution front is employed such that the interface is always located at $y = 0$ (see Fig. 1). In this coordinate system, the transverse component of the velocity at the solid surface is no longer zero but has a value equal to the local dissolution velocity, v_0. One major objective of the present study is to determine the

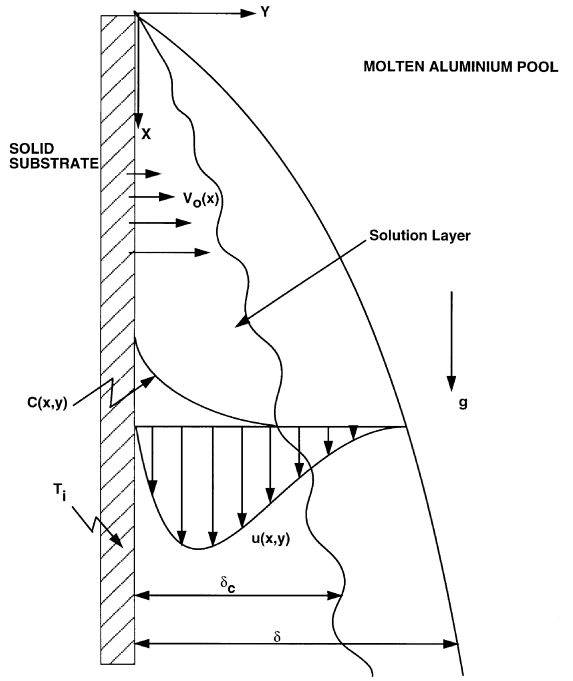

Fig. 1. A schematic of the dissolution boundary layer configuration in an isothermal binary metallic system.

axial variation of v_0 as a function of the system parameters.

For an isothermal binary metallic system, the local and the ambient densities of the fluid can be expressed by

$$\rho = \rho_m[1-(1-\rho_m/\rho_w)C]^{-1} \tag{1a}$$

$$\rho_\infty = \rho_m[1-(1-\rho_m/\rho_w)C_\infty]^{-1} \tag{1b}$$

where ρ_m is the density of the molten metallic solvent, ρ_w the density of the wall (i.e. the soluble substrate), ρ_∞ the ambient fluid density corresponding to the ambient pool concentration C_∞, and C the local mass fraction of the substrate in the solution layer. Without loss of generality, ρ_w is taken to be larger than ρ_m. In this study, the metallic solvent is taken to be aluminum. Assuming a steady, two-dimensional, laminar boundary flow, the continuity equation can be written as

$$\frac{\partial}{\partial x}(\rho u)+\frac{\partial}{\partial y}(\rho v) = 0 \tag{2}$$

where (u, v) are the velocity components in the streamwise and transverse directions, (x, y), respectively. For a concentration-driven flow, the streamwise momentum equation can be written as [2]

$$\rho u\frac{\partial u}{\partial x}+\rho v\frac{\partial u}{\partial y} = \mu\frac{\partial^2 u}{\partial y^2}+(\rho-\rho_\infty)g \tag{3}$$

where μ is the viscosity of the fluid, g the acceleration due to gravity, and ρ the local density of the solution given by eqn (1). From the conservation of species, the mass fraction is governed by the following concentration eqn [2]

$$u\frac{\partial C}{\partial x}+v\frac{\partial C}{\partial y} = D\frac{\partial^2 C}{\partial y^2} \tag{4}$$

where D is the mass diffusivity of the binary system. Note from eqn (1) that the local density is a strong function of the local concentration. Hence the local density variation has to be accounted for in the continuity equation, i.e. eqn (2).

The coordinate system is chosen to move with the dissolution front such that the solid surface is always located at $y = 0$. Relative to this coordinate system, the initial and boundary conditions are

$$x = 0 \quad \text{or} \quad y\to\infty : u = 0, C = C_\infty \tag{5a}$$

$$y = 0 : u = 0, C = C_s \tag{5b}$$

$$v = -\frac{D}{1-C_s}\frac{\partial C}{\partial y}\bigg|_{y=0} = v_0 \tag{5c}$$

where C_s is the saturated concentration at the solid/liquid interface. The term $(1-C_s)^{-1}$ in the denominator of eqn (5c) represents the induced flow correction for the transverse component of the liquid velocity at the interface (see Burmeister [9]). Note that with respect to the moving coordinate system, the transverse velocity at the solid surface is not zero but has a value equal to the dissolution velocity, v_0.

The value of C_s in eqn (5b) is a function of the interface temperature, T_i, which is taken to be the same as the system temperature. The system temperature is treated as a parameter in this study. Using the experimental data for the solubility of metals in molten aluminum at high temperatures [10, 11] and following the thermodynamic form proposed by Liu et al. [12], the saturated concentration correlation can be obtained by data fitting using the least squares technique as

$$\ln C_s = A_1/T_i+B_1 \tag{6}$$

where C_s is in wt%, T_i is in degrees Kelvin, and A_1, B_1 are constants. Equation (6) is similar to the Arrhenius equation discussed by Yeremenko et al. [13]. The constants A_1 and B_1 for various aluminum alloys are given in Table 1. For a given value of T_i, the above expression will be used to determine the saturated concentration at the interface.

The diffusion coefficient, D, plays an important role in the natural convection mass transfer process under consideration. Thus, it is necessary to determine D as a function of the system temperature, T_i. From the exper-

Table 1
Solubility constants and diffusion coefficients for metals in molten aluminum over the temperature range of 1000–1200 K

	Solubility constants		Diffusion coefficients	
Metals	A_1	B_1	A_2	B_2
Iron (Fe)	-7.74×10^3	8.89	-3.12×10^3	−16.32
Nickel (Ni)	-6.87×10^3	9.35	-5.09×10^3	−14.42
Molybdenum (Mo)	-1.32×10^4	12.00	-4.73×10^3	−15.16

imental data of Eremenko [11], the following correlation equation is obtained:

$$\ln D = A_2/T_i + B_2 \tag{7}$$

where D is in $m^2\,sec^{-1}$, T_i is in degrees Kelvin, and A_2, B_2 are constants. In eqn (7), A_2 is generally treated as the activation energy of the diffusion process and B_2 a frequency factor [14]. The constants A_2 and B_2 for various aluminum alloys are also given in Table 1.

The density, ρ_m, of molten aluminum can be determined as a linear function of temperature using the Gamma-Attenuation Technique [15]:

$$\rho_m = 2375 - 0.233(T_i - T_{mp}) \tag{8}$$

where ρ_m is in $kg\,m^{-3}$, T_i is in degrees Kelvin, and T_{mp} is the melting point of aluminum, i.e. 933.5 K. The maximum temperature of T_i in eqn (8) is 1613 K. The dynamic viscosity of molten aluminum from the results for zone-refined aluminum can be represented by the equation [10]:

$$\mu = 0.1\left[10^{((720/T_i)-2.68)}\right] \tag{9}$$

where μ is in Pa-s, T_i is in degrees Kelvin. For most aluminum alloys [10, 11], the viscosity does not vary significantly with the mass fraction. As a first approximation, μ is treated as a function of the system temperature only.

To complete the mathematical formulation of the problem, various ambient pool concentrations are considered with C_∞ being bounded between zero and the saturated value at the interface, and it can be simply related to C_s by

$$C_\infty = aC_s \qquad (0 \leqslant a \leqslant 1). \tag{10}$$

Physically, the fraction a can be viewed as the degree of saturation in the ambient fluid.

3. Analysis

The governing system, eqns (2)–(5), can be converted into a system of ordinary differential equations by invoking the following similarity transformation:

$$\eta = yGr_x^{1/4}/\sqrt{2}x \tag{11}$$

$$u = \frac{2\nu}{x} Gr_x^{1/2} \tilde{C} \frac{df}{d\eta} \tag{12}$$

$$v = \frac{\nu}{\sqrt{2}x} Gr_x^{1/4} \tilde{C}\left[\eta \frac{df}{d\eta} - 3f + \frac{V_0}{\tilde{C}_s Sc}\right] \tag{13}$$

$$\tilde{C} = 1 - (1 - \rho_m/\rho_w)C \tag{14}$$

where η is an independent similarity variable, Gr_x a local Grashof number, ν the kinematic viscosity of the fluid, $f(\eta)$ an unknown function of η to be determined in the course of analysis, $\tilde{C}_s$ a modified saturated concentration, Sc the Schmidt number of the fluid, and V_0 a dissolution constant. The expressions for Gr_x, $\tilde{C}_s$, Sc, and V_0 are given respectively by

$$Gr_x = \frac{g(1-\tilde{C}_s)x^3}{[1-a(1-\tilde{C}_s)]\nu^2} \tag{15a}$$

$$\tilde{C}_s = 1 - (1 - \rho_m/\rho_w)C_s \tag{15b}$$

$$Sc = \nu/D \tag{15c}$$

$$V_0 = [\tilde{C}_s - \rho_m/\rho_w]^{-1} \left.\frac{d\tilde{C}}{d\eta}\right|_{\eta=0}. \tag{15d}$$

In eqns (11), (13) and (15d), the axial variation of the dissolution velocity given by eqn (5c) has been properly accounted for. The quantity V_0 in equation (15d) is a true constant.

With eqns (2) and (12)–(14), the continuity equation is satisfied automatically. Equations (3) and (4) become

$$\frac{d^2}{d\eta^2}\left(\tilde{C}\frac{df}{d\eta}\right)+\left(3f-\frac{V_0}{\tilde{C}_s Sc}\right)\tilde{C}\frac{d}{d\eta}\left(\tilde{C}\frac{df}{d\eta}\right)-2\tilde{C}^2\left(\frac{df}{d\eta}\right)^2 + \frac{1-\tilde{C}}{1-\tilde{C}_s}-a=0 \quad (16)$$

$$\frac{d^2\tilde{C}}{d\eta^2}+\left(3Scf-\frac{V_0}{\tilde{C}_s}\right)\tilde{C}\frac{d\tilde{C}}{d\eta}=0. \quad (17)$$

The boundary conditions are

$$\eta=0;\quad f(0)=0,\quad f'(0)=0,\tilde{C}=\tilde{C}_s \quad (18a)$$

$$\eta\to\infty;\quad f'(\infty)=0,\tilde{C}(\infty)=1-a(1-\tilde{C}_s) \quad (18b)$$

where f' denotes the total derivatives of f with respect to η. For given values of ρ_m/ρ_w, Sc, and $\tilde{C}_s$, eqns (16) and (17) can be integrated simultaneously using the fourth order Runge–Kutta method with the initial conditions given by eqn (18) to determine the distributions of $f(\eta)$ and $\tilde{C}(\eta)$ in the dissolution boundary layer. Once $\tilde{C}(\eta)$ and is known, the dissolution constant can be calculated from eqn (15d). Note, however, that the unknown quantity V_0 also appears in eqns (16) and (17). Thus, an iterative procedure must be employed in the numerical integration of these equations. This is done by assuming an initial trial value for V_0, and the numerical iteration is carried out using the Secant shooting method. The correct value of V_0 is chosen such that eqn (15d) is satisfied. In the present numerical work, the Secant shoot method is found to be very effective in obtaining the correct value of V_0 which is independent of the initial trial value.

According to Niinomi et al. [6] and Burmeister [9], the local dissolution mass transfer coefficient is defined by

$$h_m=\frac{\rho_s v_0}{\rho_s C_s-\rho_\infty C_\infty} \quad (19)$$

where ρ_s is the fluid density at the dissolution front. Physically, $\rho_s v_0$ is the mass flux of the substrate due to dissolution and the quantity in the denominator represents the difference in the substrate concentration by volume across the dissolution boundary layer. In the present case, the ambient fluid concentration is given by eqn (10). Hence, eqn (19) can be written as

$$h_m=\left(1-\frac{\rho_\infty}{\rho_s}a\right)^{-1}\frac{v_0}{C_s} =-\left(1-\frac{\rho_\infty}{\rho_s}a\right)^{-1}\frac{D}{C_s(1-C_s)}\left.\frac{\partial C}{\partial y}\right|_{y=0} \quad (20)$$

where eqn (5c) has been employed in obtaining the above expression. The value of ρ_s is given by

$$\rho_s=\rho_m[1-(1-\rho_m/\rho_s)C_s]^{-1}. \quad (21)$$

From eqns (11), (14) and (15d), the local dissolution mass transfer coefficient is given by

$$h_m=\left(1+\frac{a\tilde{C}_s}{1-a}\right)\left(1-\frac{\rho_m}{\rho_w}\right)\frac{V_0 D}{1-\tilde{C}_s}\frac{Gr_x^{1/4}}{\sqrt{2}x}. \quad (22)$$

For a vertical substrate having a total length of L, the average dissolution mass transfer coefficient is

$$\bar{h}_m=\frac{1}{L}\int_0^L h_m\,dx. \quad (23)$$

From eqns (15a) and (22), it can be shown that

$$\bar{h}_m=\left(1+\frac{a\tilde{C}_s}{1-a}\right)\left(1-\frac{\rho_m}{\rho_w}\right)\frac{V_0 D}{1-\tilde{C}_s}\frac{2\sqrt{2}Gr_L^{1/4}}{3L} \quad (24)$$

where Gr_L is the overall Grashof number defined as

$$Gr_L=\frac{g(1-\tilde{C}_s)L^3}{[1-a(1-\tilde{C}_s)]\nu^2}. \quad (25)$$

It follows that the average Sherwood number is given by

$$\overline{Sh}=\frac{\bar{h}_m L}{D}=\left(1+\frac{a\tilde{C}_s}{1-a}\right)\left(1-\frac{\rho_m}{\rho_w}\right)\frac{2\sqrt{2}V_0 Gr_L^{1/4}}{3(1-\tilde{C}_s)}. \quad (26)$$

Note from eqns (15)–(18) that V_0 is a function of ρ_m/ρ_w, Sc, and $\tilde{C}_s$. Thus, the average Sherwood number can be correlated in the following form

$$Sh=\psi Gr_L^{1/4} \quad (27)$$

where

$$\psi=\left(1+\frac{a\tilde{C}_s}{1-a}\right)\left(1-\frac{\rho_m}{\rho_w}\right)\frac{2\sqrt{2}V_0}{3(1-\tilde{C}_s)}=\psi\left(\frac{\rho_m}{\rho_w},a,Sc,\tilde{C}_s\right). \quad (28)$$

The functional form of ψ will be determined by correlating the present numerical results.

4. Results and discussion

Numerical calculations have been performed for three aluminum alloys over the temperature range of 1000 K $\leqslant T_i \leqslant$ 1200 K for which the value of ρ_m/ρ_w varies from 0.23 to 0.3, the Schmidt number varies approximately from 46 to 202, the saturated concentration varies from 0.0029 to 0.375, and the corresponding value of $\tilde{C}_s$ varies from 0.722 to 0.998. Typical results are given in Table 2 for $T_i = 1000$ K and Table 3 for $T_i = 1200$ K. For a given system temperature, eqns (16) and (17) can be integrated numerically using the Secant shooting method to determine the profiles of $f(\eta)$ and $\tilde{C}(\eta)$, from which the value of ψ can be calculated using eqns (15d) and (28).

Table 2
Numerical results for various ambient pool concentrations in different binary systems at $T_i = 1000$ K

	Binary systems		
Parameters	Al–Fe	Al–Ni	Al–Mo
Schmidt number (Sc)	129	138	202
Density ratio (ρ_m/ρ_w)	0.30	0.27	0.23
Saturated concentration (C_s)	0.0315	0.119	0.0029
Modified saturated concentration ($\tilde{C}_s$)	0.978	0.912	0.998
$a = 0$			
$f''(0)/\tilde{C}'(0)$	0.239/0.05	0.255/0.194	0.209/0.0058
η/f'_{max}	0.45/0.037	0.40/0.037	0.40/0.03
$a = 0.5$			
$f''(0)/\tilde{C}'(0)$	0.14/0.021	0.149/0.084	0.123/0.0024
η/f'_{max}	0.50/0.0257	0.50/0.0262	0.45/0.0206
$a = 0.9$			
$f''(0)/\tilde{C}'(0)$	0.041/0.0028	0.043/0.011	0.036/0.00032
η/f'_{max}	0.65/0.0107	0.65/0.0111	0.60/0.0086

The calculated velocity profiles for the Al–Mo, Al–Ni, and Al–Fe systems in the dissolution boundary layer are shown in Fig. 2(a)–(c), respectively, for the case in which the system temperature is fixed at $T_i = 1000$ K. In these figures, the mass fraction of the substrate in the free-stream is treated as a parameter ranging from the baseline value of $a = 0$ to the near-saturation value of $a = 0.9$. The peak velocity is a monotonically decreasing function of a. As the degree of saturation in the ambient pool is increased from $a = 0$ to $a = 0.9$, the peak velocity reduces for all three aluminum alloy systems. This result is evidently due to the fact that the concentration difference across the boundary layer decreases with an increasing value of a, thus giving rise to a smaller induced velocity. For a given ambient pool concentration, the peak velocity as well as the velocity gradient at the dissolution front

Table 3
Numerical results for various ambient pool concentrations in different binary systems at $T_i = 1200$ K

	Binary systems		
Parameters	Al–Fe	Al–Ni	Al–Mo
Schmidt number (Sc)	59.4	45.8	71.1
Density ratio (ρ_m/ρ_w)	0.29	0.26	0.23
Saturated concentration (C_s)	0.114	0.375	0.0263
Modified saturated concentration ($\tilde{C}_s$)	0.919	0.722	0.980
$a = 0$			
$f''(0)/\tilde{C}'(0)$	0.31/0.14	0.44/0.38	0.27/0.04
η/f'_{max}	0.45/0.054	0.45/0.071	0.45/0.048
$a = 0.5$			
$f''(0)/\tilde{C}'(0)$	0.18/0.062	0.25/0.18	0.16/0.017
η/f'_{max}	0.55/0.038	0.55/0.051	0.55/0.033
$a = 0.9$			
$f''(0)/\tilde{C}'(0)$	0.051/0.0084	0.069/0.026	0.046/0.0022
η/f'_{max}	0.75/0.016	0.80/0.022	0.75/0.014

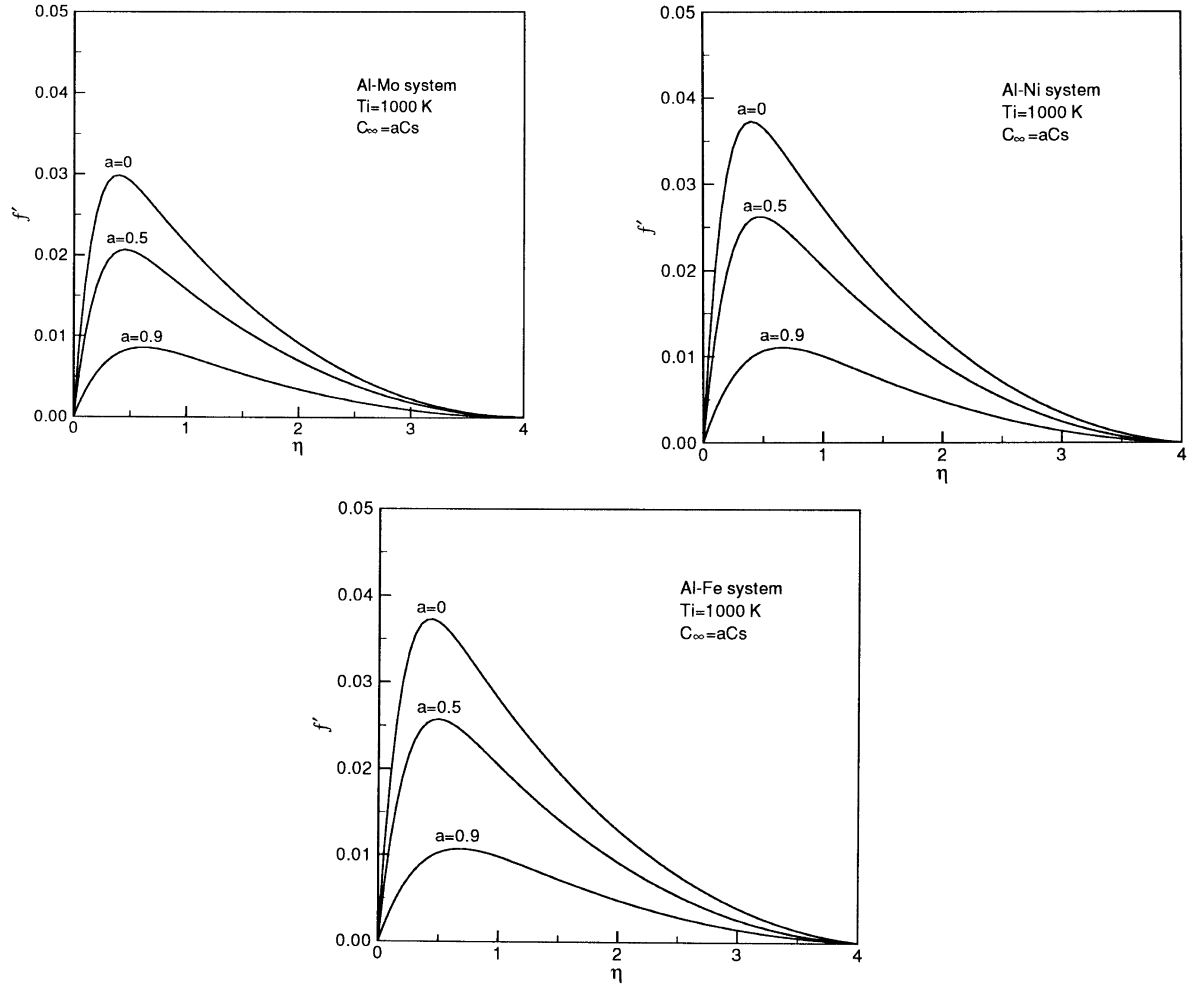

Fig. 2. (a) Modified axial velocity profiles for an aluminum–molybdenum (Al–Mo) system in the dissolution boundary layer at 1000 K for various freestream concentrations; (b) modified axial velocity profiles for an aluminum–nickel (Al–Ni) system in the dissolution boundary layer at 1000 K for various freestream concentrations; (c) modified axial velocity profiles for an aluminum–iron (Al–Fe) system in the dissolution boundary layer at 1000 K for various freestream concentrations.

vary from one aluminum alloy system to another, evidently due to the effects of the Schmidt number and the density ratio of the binary system. This is true as long as the system temperature, T_i is fixed at a constant value. The numerical results for various ambient pool concentrations are given in Table 2.

Figure 3(a)–(c) shows the distribution of $\tilde{C}(\eta)$ in the dissolution boundary layer for the Al–Mo, Al–Ni, and Al–Fe systems. For all three systems, the values of $\tilde{C}(\eta)$ almost approach their asymptotic values at $\eta = 1$. Comparing the velocity and concentration profiles for each system, it can be seen that the location at which the velocity peaks, is within the concentration boundary layer. Physically, this behavior is quite expected since the flow is induced by buoyancy due to the concentration gradients. The local mass fraction of the substrate decreases from its saturated value at the dissolution front to the ambient pool concentration at the edge of the concentration boundary layer. As the degree of saturation in the ambient fluid is increased, the concentration gradients in the boundary layer decrease, resulting in a smaller driving force for the flow.

Figures 4 and 5 show the calculated velocity and modified concentration profiles in the dissolution boundary layer for the case in which the system is at a higher temperature of $T_i = 1200$ K. Due to space limitation, results are presented only for the Al–Ni system in these figures. A comparison of Figs 2(b) and 4 indicates that the induced velocity is larger at a higher temperature. For the case of $a = 0$, the peak velocity increases by a factor of 1.90 as the system temperature is increased from 1000 K to 1200 K. For the near-saturation case of

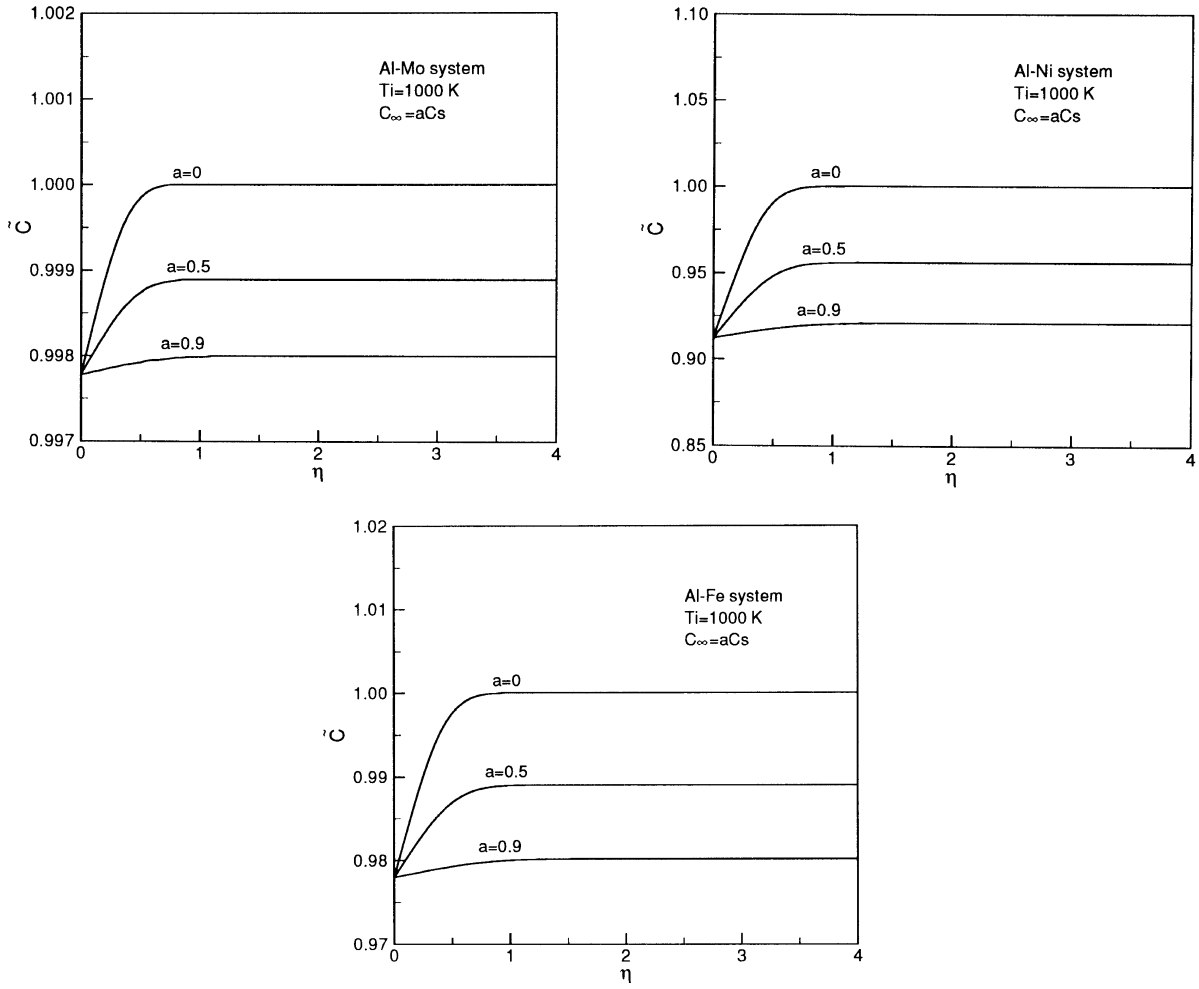

Fig. 3. (a) Distribution of the modified mass fraction of the Al–Mo alloy in the dissolution boundary layer at 1000 K for various freestream concentrations; (b) distribution of the modified mass fraction of the Al–Ni alloy in the dissolution boundary layer at 1000 K for various freestream concentrations; (c) distribution of the modified mass fraction of the Al–Fe alloy in the dissolution boundary layer at 1000 K for various freestream concentrations.

$a = 0.9$, the peak velocity increases by a factor 1.97 as the system temperature is increased from 1000 K to 1200 K. The increase in the induced velocity is evidently due to the presence of larger concentration differences across the boundary layer, as can be seen from Fig. 5. As the system temperature is increased from 1000 K to 1200 K, the saturated mass fraction of the substrate at the dissolution front increases considerably, resulting in a larger buoyancy effect. On the other hand, the thickness of the concentration boundary layer increases only moderately from 0.75 to approximately 2.0, as the saturated concentration increases much faster with temperature than does the mass diffusivity. Thus the concentration gradients increase almost by an order of magnitude within the boundary layer as the system temperature is changed from 1000 K to 1200 K, giving rise to higher local velocities. The numerical results are given in Tables 2 and 3. Note that δ is several times larger than δ_c as the Schmidt number of the fluid is much larger than unity.

For an aluminum alloy system [10, 11], ρ_m/ρ_w is approximately equal to some constant in this study. From eqns (15b) and (28), it can be shown that

$$\psi = \left[1 + \frac{a\tilde{C}_s}{1-a}\right]\frac{2\sqrt{2}V_0}{3C_s} = \psi(a, Sc, C_s). \tag{29}$$

From eqns (27) and (29) with an anticipation of $\overline{Sh} \propto Sc^{1/4}$, it may be postulated that

$$Y = \psi Sc^{1/4} = Y(a, C_s) \tag{30}$$

where $Y(a, C_s)$ is an unknown function of a and C_s. A plot of Y versus C_s is shown in Fig. 6 for the three

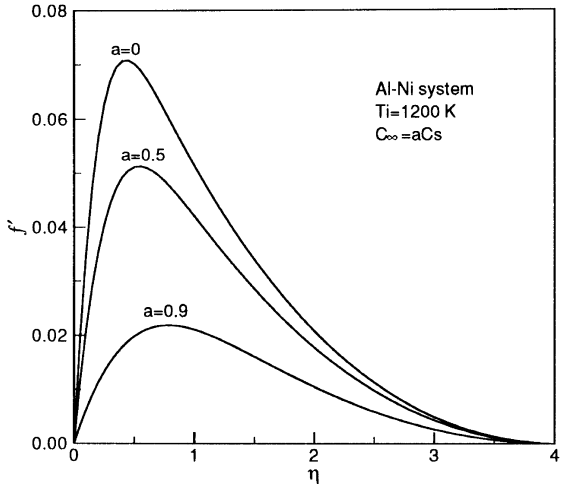

Fig. 4. Modified axial velocity profiles for an aluminum–nickel (Al–Ni) system in the dissolution boundary layer at 1200 K for various freestream concentrations.

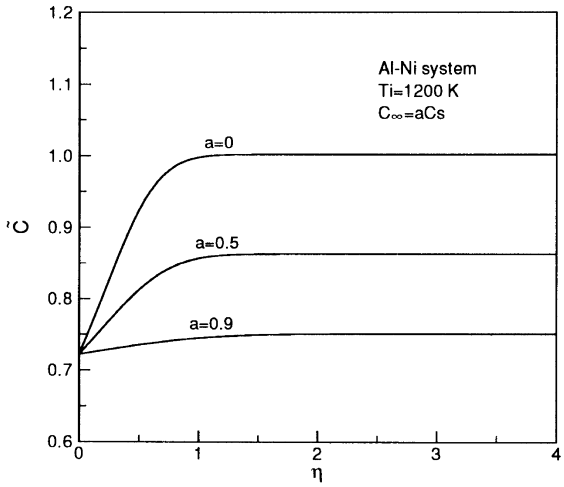

Fig. 5. Distribution of the modified mass fraction of the Al–Ni alloy in the dissolution boundary layer at 1200 K for various freestream concentrations.

aluminum alloys for various values of a. These numerical data are obtained by calculating the value of V_0 and thus the value of ψ at various system temperatures, corresponding to different sets of Sc and C_s. The fitting equation for function Y can be written as

$$Y = Y(a, C_s) = b_0 + b_1 C_s + b_2 C_s^2 \tag{31}$$

where b_0, b_1, and b_2 are coefficients dependent only on the value of a, and their corresponding values are given in Table 4. In view of the similarity among the various curves in Fig. 6, a further analysis is done by a normalization procedure. The value of Y for different alumi-

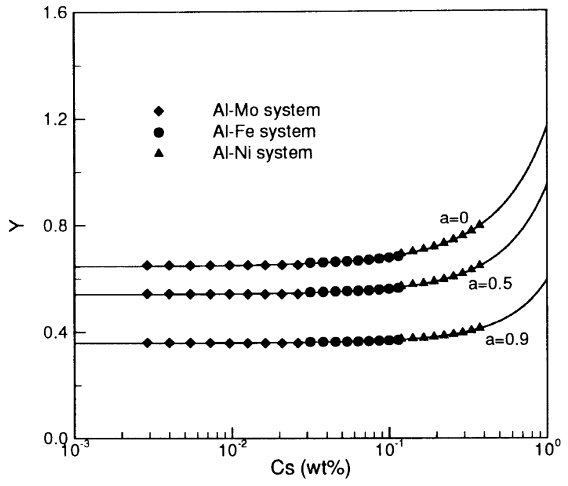

Fig. 6. Correlation of the numerical data for various metals in molten aluminum.

Table 4
Correlation equation constants for various ambient pool concentrations

Ambient pool concentrations	Constants		
	b_0	b_1	b_2
$a = 0$	0.647	0.332	0.190
$a = 0.5$	0.541	0.201	0.208
$a = 0.9$	0.0358	0.090	0.147

num alloy systems is divided by the coefficient b_0 at various values of a, and then plot against C_s for all three aluminum systems as shown in Fig. 7. By correlating the numerical data, a parabolic curve is obtained over the range $0.0029 \leqslant C_s \leqslant 0.375$ where

$$Y/b_0 = 1 + 0.38C_s + 0.36C_s^2. \tag{32}$$

Since b_0 is only dependent on the value of a, a reasonable linear correlation can be done as in Fig. 8. The equation is correlated as

$$b_0 = 0.66 - 0.32a. \tag{33}$$

From eqns (27, 31, 33, 34), a correlation for the average Sherwood number can be obtained. This is

$$\overline{Sh} = (0.66 - 0.32a)(1 + 0.38C_s + 0.36C_s^2)Sc^{1/4}Gr_L^{1/4}. \tag{34}$$

The above result indicates that the average dissolution mass transfer coefficient for binary metallic system is a function of both the saturated concentration of the substrate at the solid/liquid interface and the degree of

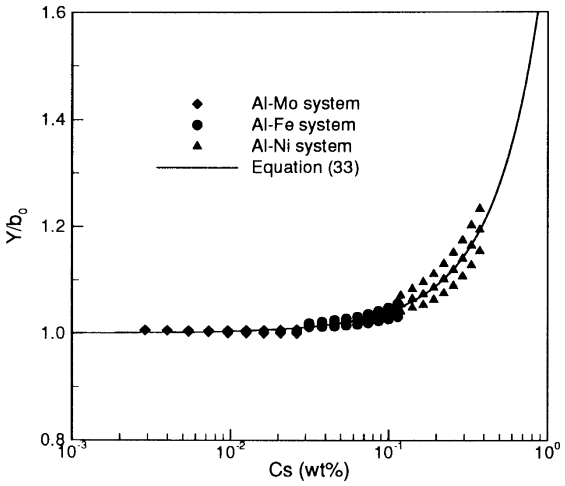

Fig. 7. Correlation of the normalized data for various metals in molten aluminum.

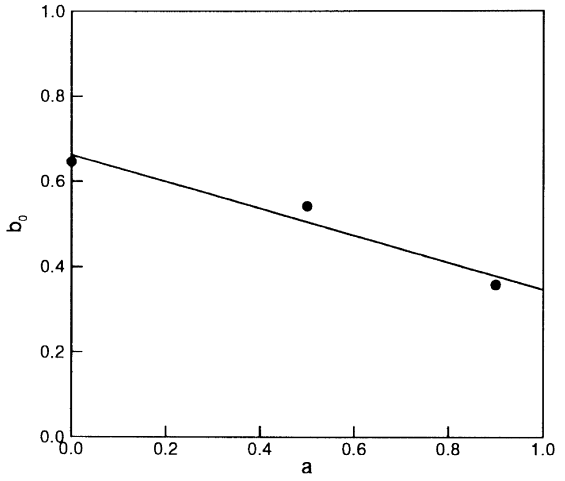

Fig. 8. Correlation of the coefficient b_0 for different values of a.

saturation in the ambient pool. It should be noted that at the limits of $a \to 0$ and $C_s \to 0$, eqn (34) reduces to

$$\overline{Sh}_0 = 0.66 Sc^{1/4} Gr_L^{1/4} \tag{35}$$

which is identical to the classical result reported for natural convection heat transfer analogy [16].

5. Conclusions

A physical model has been developed to describe the process of dissolution mass transfer in an isothermal binary metallic system. Based upon the results of the present study, the following conclusions can be made.

1. The flow induced by the dissolution process is a strong function of the ambient pool concentration as well as the system temperature. This is due to the fact that the solubility of the wall material given by the phase diagram of the binary system is uniquely determined by the system temperature. A higher velocity is induced as the system temperature is increased.
2. For given ambient pool concentration and system temperature, the peak velocity induced in the dissolution boundary layer as well as the velocity gradient in the dissolution front vary from one aluminum alloy system to another, evidently due to the effects of the Schmidt number and the density ratio of the binary system.
3. The momentum boundary layer is several times thicker than the concentration boundary layer. This is typical for molten metallic systems whose Schmidt numbers are usually much larger than unity.
4. The average Sherwood number not only depends on the Grashof number and Schmidt number but is also a strong function of the saturated concentration of the substrate at the dissolution front and the degree of saturation in the ambient pool. Over the range of $0.0029 \leqslant C_s \leqslant 0.375$, the average Sherwood number can be correlated to these four controlling parameters in the form given by eqn (34).
5. The classical result reported for natural convection heat transfer analogy [16] can be obtained as a limiting case of the present study with $a \to 0$ and $C_s \to 0$, as given by eqn (35).

References

[1] Cheung FB, Yang BC, Li D, Cho DH, Tan MJ. Effects of freestream velocity and concentration on dissolution mass transport in a steel/aluminum system. AIChE Symposium Series 1993;89:396–403.
[2] Gebhart B, Jaluria Y, Mahajan RL, Sammakia R. Buoyancy-Induced Flows and Transport, Hemisphere, New York, 1988, Chap. 6.
[3] Ravoo E, Rotte JW, Sevenstern FW. Theoretical and electrochemical investigation of free convection mass transfer at vertical cylinders. Chemical Engineering Science 1970;25:1637–52.
[4] Gairola PK, Tiwari RK, Ghosh A. Rates of dissolution of a vertical nickel cylinder in liquid aluminum under free convection. Metallurgical Transactions 1971;2:2123–6.
[5] Niinomi M, Ueda Y, Sano M. Dissolution of ferrous alloys into molten aluminum. Transactions of the Japan Institute of Metals 1982;23:780–7.
[6] Niinomi M, Suzuki Y, Ueda Y. Dissolution of ferrous alloys into molten pure aluminum under forced flow. Transactions of the Japan Institute of Metals 1984;25:429–39.

[7] Niinomi M, Ueda Y. On the alloy layers formed by the reaction between ferrous alloys and molten aluminum. Transactions of the Japan Institute of Metals 1982;23:709–17.
[8] Dybkov VI. Interaction of 18Cr–10Ni stainless steel with liquid aluminum. Journal of Materials Science 1990;25:3615–33.
[9] Burmeister LC. Convective Heat Transfer, 2nd edn, Wiley, New York, 1993, p. 206.
[10] Hatch JE. Aluminum : Properties and Physical Metallurgy, American Society for Metals, Metals Park, 1984, pp. 17, 26.
[11] Eremenko VN, Natanzon YaV, Dybkov VI. Physico-chemical processes on the solid metal–molten metal interface. Soviet Materials Science (Translated from Fiziko-Khimicheskaya Mekhanika Materialov) 1984;20:3–9.
[12] Liu H, Bouchard M, Zhang L. An experimental study of hydrogen solubility in liquid aluminum. Journal of Materials Science 1995;30:4309–15.
[13] Yeremenko VN, Natanzon YaV, Dybkov VI. Interaction of the refractory metals with liquid aluminum. Journal of the Less-Common Metals 1976;50:29–48.
[14] Guminski C. Diffusion coefficients in liquid metals at high dilution. In HU Borgstedt and G Frees, editors. Liquid Metal System, Plenum Press, New York, 1995, pp. 345–356.
[15] Nasch PM, Steinemann SG. Density and thermal expansion of molten manganese, iron, nickel, copper, aluminum and tin by means of the gamma-ray attenuation technique. Physics and Chemistry of Liquids 1995;29:43–58.
16. Skelland AHP. Diffusional Mass Transfer, John Wiley, New York, 1974, p. 124.